Optical Properties of Superconducting $Nd_{0.8}Sr_{0.2}NiO_2$ Nickelate

Rebecca Cervasio[1*], Luca Tomarchio[2,3*], Marine Verseils[1], Jean-Blaise Brubach[1], Salvatore Macis[2,4], Shengwei Zeng[5], Ariando Ariando[5], Pascale Roy[1] ✉, and Stefano Lupi[2,4] ✉

[*]These authors contributed equally to this work
[1]Synchrotron SOLEIL, L'Orme des Merisiers, Saint-Aubin BP 48, 91192 Gif-sur-Yvette Cedex, France
[2]Department of Physics, Sapienza University, Piazzale Aldo Moro 5, 00185, Rome, Italy.
[3]INFN section of Rome, P.Le Aldo Moro, 2, 00185 Rome, Italy.
[4]INFN - Laboratori Nazionali di Frascati, via Enrico Fermi 54, 00044, Frascati (Rome), Italy.
[5]Department of Physics, Faculty of Science, National University of Singapore, Singapore 117551, Singapore
✉e-mail: stefano.lupi@uniroma1.it, pascale.roy@synchrotron-soleil.fr

ABSTRACT

The intensive search for alternative non-cuprate high-transition-temperature (T_c) superconductors has taken a positive turn recently with the discovery of superconductivity in infinite layer nickelates[1]. This discovery is expected to be the basis for disentangling the puzzle behind the physics of high T_c in oxides. In the unsolved quest for the physical conditions necessary for inducing superconductivity, we report an optical study of a $Nd_{0.8}Sr_{0.2}NiO_2$ film measured using optical spectroscopy, at temperatures above and below the critical temperature $T_c \sim 13$ K. The normal-state electrodynamics of $Nd_{0.8}Sr_{0.2}NiO_2$, is described by the Drude model characterized by a scattering time just above T_c ($\tau \sim 1.7 \times 10^{-14}$ s) and a plasma frequency $\omega_p = 8500$ cm^{-1} in combination with an absorption band in the Mid-Infrared (MIR) around $\omega_0 \sim 4000$ cm^{-1}. The MIR absorption indicates the presence of strong electronic correlation effect in the NiO_2 plane similarly to cuprates. Below T_c, a superconducting energy gap (2Δ) of ~ 3.2 meV is extracted from the Terahertz reflectivity using the the Mattis-Bardeen model. From the Ferrel-Glover-Thinkam Rule applied to the real part of the optical conductivity, we also estimate a London penetration depth of about 490 nm, in agreement with a type-II[2] superconductivity in $Nd_{0.8}Sr_{0.2}NiO_2$ Nickelate.

Key points: Unconventional superconductivity, Nickelates, Superconducting gap, THz spectroscopy

Introduction

The complex physics behind the superconductive phase in high temperature superconductors like cuprates still shows unknown aspects nearly 35 years from their first discovery by Bednorz and Mueller[3]. Since then, the search for the pairing mechanism in cuprates has been a major research focus. To explore this mechanism, additional high-T_c superconductors families were searched for, with different transition metals but similar crystal and electronic structures[4,5]. One such family, the nickelates, is built from 2D planes of NiO_2 interchanged with dopant ions that form spacer layers, equivalent to the CuO_2 planes in cuprates. A superconductive phase was recently verified experimentally more than 20 years after their first theoretical prediction[6] in Sr-doped $NdNiO_2$ thin films grown on STO substrates.

The infinite-layer nickelate, $Nd_{0.8}Sr_{0.2}NiO_2$, is synthesized via softchemistry topotactic reduction[7] on a STO substrate reaching a type-II superconductive phase with a relatively high-transition temperature of about 9-15 K[1]. The presence of the STO substrate is essential for producing the superconductive phase, giving an unusual picture in which the substrate both strains the crystal and stabilizes this phase. As for other unconventional superconductors, the superconductivity is induced by charge doping in the parent compound. Although the phase diagram of $Nd_{1-x}Sr_xNiO_2$ shows a superconductive dome, with the highest critical temperature (of about 15 K) at Sr doping $x = 0.2$[8], nickelates reveal many differences with respect to cuprates. The most noticeable distinction is that no evidence of magnetic ordering is experimentally observed[1,7,8]. Moreover, Hall measurements[1] and ab-initio simulations[9–13] highlighted a complex picture behind the symmetry of the order parameter, in which the superconductive mechanism appears inconsistent with the picture of a simple hole doped electronic band. Indeed, the description of the electronic structure near the Fermi level might require up to three bands and their hybridization[14], and contributions coming from the 4*f* shells have also been proposed[15]. Furthermore, the role of electronic correlations has been pointed-out recently[16], although an estimate of their importance is still lacking. On the other hand, the electron-phonon coupling

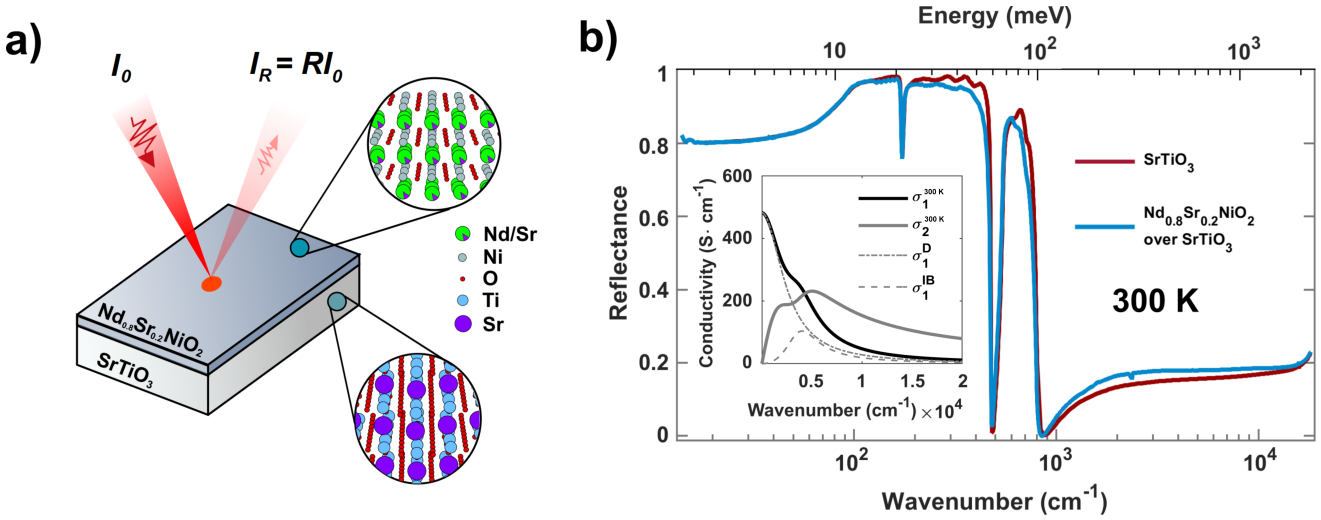

Figure 1. | Reflectance spectroscopy of a $Nd_{0.8}Sr_{0.2}NiO_2$/STO thin film. a) Schematic view of $Nd_{0.8}Sr_{0.2}NiO_2$/STO thin film sample and incoming I_0 and reflected light intensity $I_R = RI_0$ (R is the reflectance). Crystal structures are represented in the magnification circles. **b)** Broadband reflectance spectra of $Nd_{0.8}Sr_{0.2}NiO_2$/STO thin film (light blue line) and STO substrate (red line) at room temperature. The real (σ_1) and imaginary (σ_2) part of the film's optical conductivity at 300 K are plotted in the inset together with the (σ_1^D) Drude (dashed-dotted line) and (σ_1^{IB}) Mid-IR band (dashed line) fitting results.

has been ruled out as the exclusive origin of the observed superconductivity[14], with spin fluctuations playing a key role despite the absence of long-range magnetic order[13,17].

To determine the superconducting gap (2Δ) and the pairing mechanism of the superconducting state, Terahertz (THz) or microwave absorption spectroscopy[18–20], tunneling spectroscopy[21], specific heat[22,23], and London penetration depth techniques are the prevailing experimental methods. In the case of $Nd_{1-x}Sr_xNiO_2$, London penetration depth measurements produce consistent data between different independent reports[24,25], but the paramagnetic background and limited quality of the samples leave the interpretation open for further debate. Moreover, tunneling measurements on $Nd_{1-x}Sr_xNiO_2$ were also performed[26], suggesting the presence of two different superconducting gaps at 3.9 meV and 2.35 meV.

On the other hand, no optical investigations of superconductive $Nd_{0.8}Sr_{0.2}NiO_2$ films were reported, due in part to the presence of the $SrTiO_3$ substrate, reflecting close to 100% of the THz light through its soft phonon mode. Since optical investigations contributed a great deal to shed light on high temperature superconductivity mechanism through evaluations of the superconductive gap, the penetration depth, the scattering mechanism and coherence effects[27–32], these measurements are highly longed for.

In the present study, we report on the optical reflectance R(ω) of the optimally doped $Nd_{0.8}Sr_{0.2}NiO_2$ film over an STO substrate across a broad range of frequencies ω, from Terahertz (THz) to Ultraviolet (UV), as obtained by combining THz radiation, generated from the AILES beamline@Soleil third generation synchrotron machine, with conventional optical spectroscopy. The normal-state optical conductivity, derived from these measurements, is described by a superposition of a Drude term and an absorption band in the Mid-IR. This scenario is common to other metallic oxides including cuprates and suggests an important role of electronic correlations in the NiO_2 plane. In the superconducting state, the energy gap (2Δ) is evaluated by fitting the THz reflectance at different temperatures with the Mattis-Bardeen model. We extract the superconducting gap values as a function of temperature and we estimate the magnetic penetration depth through the study of the Drude spectral weight transfer to the Cooper pairs.

Experimental Results

All reflectance measurements were performed on a 10 nm thick, optimally doped $Nd_{0.8}Sr_{0.2}NiO_2$ film, grown on a 500 μm $SrTiO_3$ (STO) (001) substrate, through the soft chemistry topotactic reduction using CaH_2 (see Methods). The optical properties of the actual STO substrate have been measured in the same experimental conditions. The infinite layer structure of $Nd_{0.8}Sr_{0.2}NiO_2$ and the perovskite structure of STO are represented in Fig. 1a. Prior to optical measurements, superconductivity was verified by resistance measurements as a function of temperature, showing a $T_c \simeq 13$ K (see Figure S1 in Supplementary Information).

The optical reflectance measured at room temperature is shown in Fig. 1b, across a wide range of frequencies, from THz

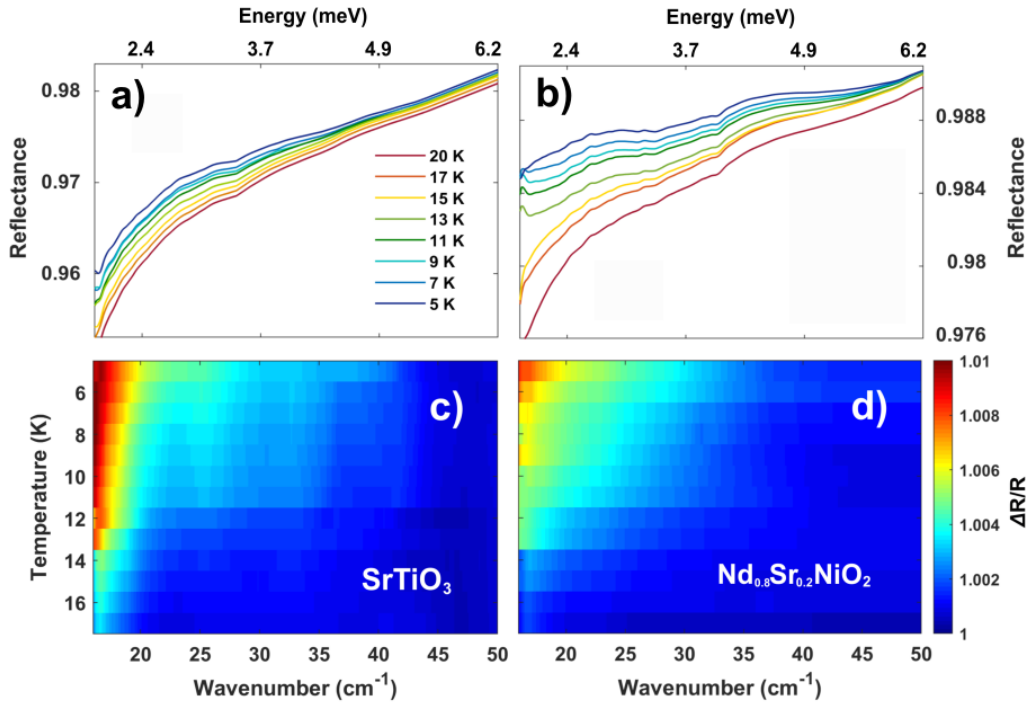

Figure 2. | **Temperature dependent analysis of a $Nd_{0.8}Sr_{0.2}NiO_2$/STO THz reflectivity. a)** THz reflectance of the STO substrate at different temperatures. At frequencies ($\omega > 50$ cm^{-1}) the curves merge toward a common absolute value. **b)** Absolute THz reflectance of the sample at different temperatures. **c-d)** Contour plots of the relative THz reflectance for both the bare substrate and sample, as a function of temperature (5 to 20 K) and frequency. Spectra were divided by measurement at 20 K.

to UV for both $Nd_{0.8}Sr_{0.2}NiO_2$ film and STO substrate. A gold layer evaporated on both film and substrate has been used as a reference for absolute measurements. For the STO substrate, a series of strong transverse optical (TO) phonon modes is observed. Starting from lower frequencies, these can be identified as[33,34]: TO_1 at 100 cm^{-1} (soft mode), TO_2 at 176 cm^{-1} and TO_3 at 540 cm^{-1}. The reflectance of $Nd_{0.8}Sr_{0.2}NiO_2$ film shows a similar behavior of STO with a small decrease above 200 cm^{-1}, mainly related to the Drude metallic absorption, and an increase above 1000 cm^{-1} associated to an absorption band in the infrared spectral region (see discussion of Eq.1).

THz reflectance measurements of film and substrate have also been performed as a function of temperature between 5 to 20 K, crossing for the film its superconductive critical temperature at $T_c \sim 13$ K and in the frequency range 15 to 50 cm^{-1} (all curves at different T merge above this frequency). Figure 2a shows the STO reflectance in this temperature and frequency range in a very expanded vertical scale. The increase in the substrate reflectance at low frequencies is due to the STO soft mode. This well known effect is further highlighted in Fig. S2 of supplementary material. In contrast, R(ω) of the film in the same temperature and frequency range (Fig. 2b) shows a larger red shift suggesting a further effect induced by the superconducting transition.

To magnify this effect, we calculate the relative reflectance spectra $\Delta R/R = (I_R(T) - I_R(20K))/I_R(20K)$ as obtained by dividing the light intensity reflected by the film or STO ($I_R(T)$) at all temperatures by the signal ($I_R(20K)$) at the reference temperature $T = 20$ K ($> T_c$). The results are shown in a 2D intensity-plot for STO and $Nd_{0.8}Sr_{0.2}NiO_2$ film (Fig. 2c,d, respectively) as a function of both temperature and frequency (the same results are shown as 3D plots in Fig. S3 of SI) . The 2D plots clearly highlight the differences between the bare substrate and the film Terahertz properties *vs*. T, supporting a different origin for the modification of the reflectance spectra at the lowest temperatures.

Discussion of Results

Normal State Optical Conductivity

To analyse the behaviour of the $Nd_{0.8}Sr_{0.2}NiO_2$ film, it is necessary to consider the optical response of the substrate. To do so, the substrate optical data were analysed through a Kramers-Kronig constrained fitting to extract the optical refraction index at every temperature[35]. Therefore, $Nd_{0.8}Sr_{0.2}NiO_2$ film are modeled in terms of an air/STO/film/air quadrilayer[36] and fitted

through the RefFit program[35]. In particular, the optical properties of $Nd_{0.8}Sr_{0.2}NiO_2$ have been described in the normal state in terms of a Drude-Lorentz model. The complex conductivity expressed in units of $S \cdot cm^{-1}$ takes the form[37]

$$\sigma(\omega) = \frac{2\pi}{Z_0}\frac{\omega_p^2}{\Gamma - i\omega} + \frac{2\pi}{Z_0}\frac{\omega\omega_{pL}^2}{\gamma\omega - i(\omega_0^2 - \omega^2)} \tag{1}$$

where Z_0 is the free space impedance (377 Ω) and the frequencies are expressed in units of cm^{-1}. In the Drude term, ω_p is the Drude plasma frequency while $\Gamma = 1/\tau$ is the scattering rate, with τ being the scattering time. The Lorentz oscillator is instead described by its characteristic frequency (ω_0) and intensity (ω_{pL}^2) and scattering rate γ. In the fitting procedure, the real (n) and imaginary (k) parts of STO refraction index have been used as inputs together with its thickness, taking into account the contribution to the reflectance coming from the substrate layer.

The inset of Fig. 1b shows the real ($\sigma_1(\omega)$, black line) and imaginary part ($\sigma_2(\omega)$, gray line) of the optical conductivity for the $Nd_{0.8}Sr_{0.2}NiO_2$ film in its normal-state together with the Drude term (dashed-dotted line) and the MIR band (dashed line). A Drude plasma frequency $\omega_p = 8500$ cm^{-1} is extracted from the fitting, together with a scattering time $\tau \sim 1.39 \times 10^{-14}$ s. Such a low scattering time is probably related to the quasi-2D geometry of the material. The MIR band is centered at $\omega_0 = 4000$ cm^{-1} with an amplitude $\omega_{pL} = 5000$ cm^{-1} (all fitting parameters are reported in Table S1 of SI). The MIR band is a common feature of many transitional metal oxides including cuprate- and iron-based superconductors, being related to electronic correlations. These usually renormalize the Drude term (coherent charge excitations), transferring spectral weight to an incoherent one at finite frequency (MIR band)[38,39]. In particular, the $\omega_p^2/(\omega_p^2 + \omega_{pL}^2)$ ratio provides an experimental estimate of the degree of electronic correlation of the material[40]. While for weakly correlated metals, such as gold and silver, one obtains $\omega_p^2/(\omega_p^2 + \omega_{pL}^2) \to 1$, for $Nd_{0.8}Sr_{0.2}NiO_2$ this ratio reaches a value of about 0.74. This number can be compared to other correlated oxides like V_2O_3 (~ 0.18) and cuprates ($0.2 - 0.4$)[41], identifying $Nd_{0.8}Sr_{0.2}NiO_2$ as an intermediate correlated system. This is an important constraint for all theoretical models[16].

At lower temperatures, above the superconducting transition (at 20 K), the fitting provides similar results with a 20% increase in the Drude scattering time, as expected for a coherent metallic transport. With the scattering time value at 20 K ($\tau \sim 1.7 \times 10^{-14}$ s), it is possible to estimate whether the nickelate is in a clean limit for superconductivity ($\hbar/\tau \ll 2\Delta$) or in the dirty one ($\hbar/\tau \approx 2\Delta$). As an initial assumption, we may take the $2\Delta = 3.9\,meV$ value as a reference for the superconductive gap, as obtained by tunneling spectroscopy measurements[26]. By calculating the ratio $\hbar/2\Delta = 1.7 \times 10^{-13}\,s$ and comparing it with the scattering time τ, we obtain $\tau < \hbar/2\Delta$. This result suggests that the material is in the dirty limit, granting the possibility to extract the superconducting gap from optical measurements.

The scattering time τ can be also related to the critical temperature T_c of the superconductor through the well known relation $\hbar/\tau \approx 2k_BT_c$, which is valid for cuprate high temperature superconductors, both in the bulk[37] and thin film limit[42]. This relation finds its origin in the scaling factor for cuprates proposed by Homes et al.[43,44] and supported by Tallon et al.[45], in which the normal state conductivity is established to be proportional to the product of the superfluid density with T_c. The result for the nickelate film, however, strongly departs from this relationship. Indeed, $\hbar/\tau$ is more than one order of magnitude higher than $2k_BT_c$: $\hbar/\tau \sim 38.7\,meV \gg 2.2\,meV \sim 2k_BT_c$. Some of the physical phenomena suggested as origin to this scaling relation in cuprates[45] are a marginal Fermi-liquid state, Josephson coupling between planes, the scattering of impurities for a d-wave order parameter and even a BCS dirty limit superconductivity. Thereby, an exact physical interpretation of our results seems unclear and it adds to the list of differences between the nickelate and cuprate families.

Optical Determination of the Superconducting Gap

In order to extract the superconducting gap and its temperature dependence, we fit the film relative reflectance $\Delta R/R = [R(T < T_c) - R(20\,K)]/R(20\,K)$ at various temperatures. In the dirty limit of the electron transport, the fitting process can be worked out by using the Mattis-Bardeen theory[46]. The choice of using the relative reflectance measurements for the understanding of the superconducting transition is mainly justified by to the high substrate absolute reflectance. Indeed, relative measurements grant a higher sensitivity when comparing different temperatures, and the use of the Mattis-Bardeen theory for the study of superconductive materials is well documented[47–49]. The real $\sigma_1^{sc}(\omega)$ and imaginary $\sigma_2^{sc}(\omega)$ parts of the optical conductivity in the superconducting state, normalized to those of the normal state $\sigma_N(\omega)$, take the form[46]

$$\frac{\sigma_1^{sc}}{\sigma_N} = \left(1 + \frac{2\Delta}{\hbar\omega}\right)E(p) - 2\left(\frac{2\Delta}{\hbar\omega}\right)K(p) \qquad (\hbar\omega > 2\Delta) \tag{2}$$

$$\frac{\sigma_2^{sc}}{\sigma_N} = \frac{1}{2}\left\{\left(\frac{2\Delta}{\hbar\omega} + 1\right)E(p') + \left(\frac{2\Delta}{\hbar\omega} - 1\right)K(p')\right\} \tag{3}$$

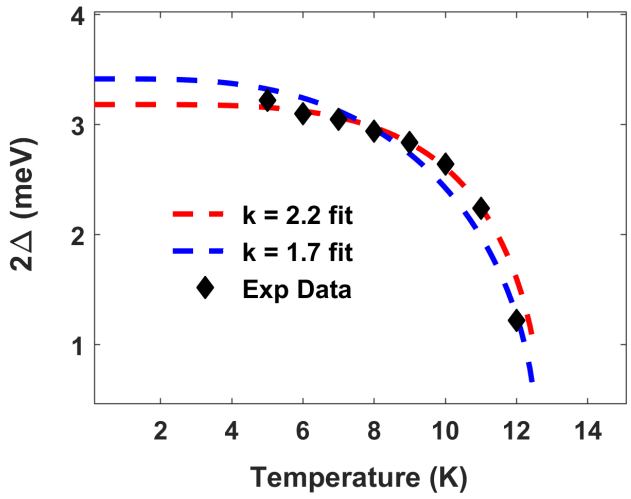

Figure 3. | Superconducting gap of $Nd_{0.8}Sr_{0.2}NiO_2$ superconductive film. Superconducting gap value (black diamond) as function of temperature. The experimental data can be described by Eq. 4 (see text) where the coupling constants $k = 2.2$ (red-dashed line) corresponds to a 2D d-pairing while $k = 1.7$ (blue-dashed line) corresponds to an s-wave pairing. In both cases, the gap extrapolation to 0 K gives a value around 3 meV.

where σ_N is mostly dominated by its real part at THz frequencies. For frequencies $\hbar\omega \leq 2\Delta$, the real part σ_1^{sc} is identically zero. $E(p)$ and $K(p')$ are the elliptical integrals of second and first kind, while the arguments p and p' take the form

$$p = |2\Delta - \hbar\omega|/|2\Delta + \hbar\omega|, \qquad p' = \sqrt{1-p^2}$$

The best fit provides the value of the superconducting gap 2Δ whose behavior vs. T is shown in Fig. 3. Here, 2Δ opens at T_c in agreement with the resistance measurements (see Fig. S1 in SI) and previous studies[1,8] and rapidly increases for reducing T. In order to extrapolate 2Δ at 0 K, we fit its T-dependence through the following equation[31,50]

$$2\Delta(T) = 2\Delta(0)\tanh\left(k\sqrt{\frac{T_c}{T}-1}\right) \tag{4}$$

where k is a coupling constant, T_c the critical temperature and $2\Delta(0)$ the superconducting gap at 0 K. Two options for the coupling constant values have been considered: 2.2 (red-dashed line in Fig. 3), and 1.7 (blue-dashed line in Fig. 3), which can be associated to a two-dimensional d-wave pairing mechanism and to a s-wave coupling, respectively[51]. Using $k = 2.2$, the extrapolation at 0 K gives $2\Delta(0)$ of 3.18 meV, while for $k = 1.7$ a slightly higher value of 3.42 meV is obtained. If instead the value of $T_c \sim 13\ K$ is fixed in Eq. 4 performing the fit, the values $k = 1.78 \pm 0.19$ and $2\Delta(0) = 3.31 \pm 0.14\ meV$ are obtained. Both values are, nonetheless, in agreement with the high-energy gap as obtained from tunneling measurements[26]. However, due to the strong contribution of the substrate to the reflectance measurements, the uncertainty of the superconducting gap extrapolation is too high to distinguish between the different coupling mechanisms (s-wave, d-wave or multigap superconductivity), proposed for nickelates[24,25].

Another fundamental quantity characterizing the superconducting state is the London penetration depth λ_L. This quantity can be estimated from the Ferrel-Glover-Thinkam Rule[52], describing the partial transfer of the Drude spectral weight to the superconducting condensate. This shift is schematically reported in Fig. S4 of the SI. The London frequency ω_L (expressed in cm^{-1}) can be calculated by the following equation[53]

$$\omega_L^2 = \frac{Z_0}{\pi}\int_0^{\omega_c}[\sigma_N(\omega') - \sigma_1^{sc}(\omega')]d\omega' \tag{5}$$

where the integral converges when performed up to a frequency cutoff $\omega_c \simeq 500\ cm^{-1}$ containing the whole Drude spectral weight. From ω_L, it is possible to calculate the penetration depth $\lambda_L = 1/2\pi\omega_L$[53]. The optical value for the penetration depth estimation at low temperature, $\lambda_L(5\ K) \simeq 490$ nm, is in agreement with results obtained with other techniques[24,54].

From a theoretical point of view, Bernardini et at.[55] reported a Density Functional Theory (DFT) calculation suggesting that electronic anisotropy is very high in $Nd_{0.8}Sr_{0.2}NiO_2$. The predicted values for λ_L range from 57 to 290 nm depending on

the crystallographic direction and the state intercepting the Fermi level (hole or electron pocket). The largest value of λ_L for the β' electron pocket ($\sim$ 290 nm) is in reasonable agreement with the London penetration depth value determined in this study ($\sim$ 490 nm). As in the β' participates the Nd-4f state, this suggests a multigap nature of the pairing mechanism in $Nd_{0.8}Sr_{0.2}NiO_2$. The discrepancy between the theoretical and our estimated values, however, may come from the ideal bulk material and the absence of the correlations used in the simulation.

Conclusion

In this manuscript, we investigated the low-energy electrodynamics of the novel nickelate $Nd_{0.8}Sr_{0.2}NiO_2$ superconducting thin film by using broad-band optical spectroscopy from Terahertz to Visible. In analogy with most High-T_c cuprates, the normal-state electrodynamics of $Nd_{0.8}Sr_{0.2}NiO_2$ can be described by the Drude model characterized by a scattering time $\tau \sim 1.7 \times 10^{-14}$ s and a plasma frequency $\omega_p = 8500$ cm^{-1} in combination with an Mid-IR absorption band at about $\omega_0 = 4000$ cm^{-1} with an amplitude of $\omega_{pL} = 5000$ cm^{-1}. The $\omega_p^2/(\omega_p^2 + \omega_{pL}^2) = 0.74$ ratio can be used to estimate the degree of electronic correlation in $Nd_{0.8}Sr_{0.2}NiO_2$[40], setting the nickelate infinity layer family in an intermediate level of correlation, well above the strong correlation values (0.2 – 0.4) corresponding to cuprates[41]. Moreover, the scaling law ($\hbar/\tau \sim 2k_BT_c$) valid for High-T_c cuprates[37] is not satisfied by the $Nd_{0.8}Sr_{0.2}NiO_2$ superconductor ($\hbar/\tau \sim 38.7\ meV \gg 2.2\ meV \sim 2k_BT_c$). This indicates a further difference among charge fluctuations in the CuO_2 and NiO_2 planes. Below T_c, through the Mattis-Bardeen model, we extract from the Terahertz optical data a superconducting gap $2\Delta \sim 3.2$ meV together with a London penetration depth of nearly 490 nm at 5 K, finally suggesting a dirty-limit type-II superconductivity in $Nd_{0.8}Sr_{0.2}NiO_2$.

Methods

Sample Preparation

We prepared and characterized our $Nd_{0.8}Sr_{0.2}NiO_3$ thin film samples following procedures previously described by Zeng et al.[8] The perovskite $Nd_{0.8}Sr_{0.2}NiO_3$ thin films with thickness of 10 nm were grown on a TiO_2-terminated (001) $SrTiO_3$ (STO) substrate using a pulsed laser deposition (PLD) technique. The deposition temperature, oxygen partial pressure P_{O_2} and laser energy density were set to be 600 °C, 150 mTorr and 1.8 J·cm^{-2}, respectively. The samples were annealed for 10 min at 600 °C and 150 mTorr after deposition, and then cooled down to room temperature at a rate of 8 °C/min. The infinite-layer structure was obtained through a soft-chemistry topotactic reduction using CaH_2 as the reagent. During the reduction process, the perovskite films were embedded into CaH_2 powder and wrapped in aluminum foil, and then heated in PLD vacuum chamber. The samples were heated to 340–360 °C at a rate of 25 °C/min and kept for 80 minutes, and then cooled down to room temperature at a rate of 25 °C/min. In order to obtain the reflectance spectra through THz measurement, half of the infinite-layer thin film was covered by 50 nm Au layer which was deposited by evaporation.

Spectroscopic Measurements

The film optical properties from THz to VIS have been probed using a combination of different spectrometers. The THz reflectance measurements have been performed at the infrared spectroscopy beamline AILES (Advanced Infrared Line Exploited for Spectroscopy), Synchrotron SOLEIL[56]. Exploiting the high brightness of the synchrotron radiation source. THz spectra in the $10 - 600$ cm^{-1} range were obtained using a Bruker IFS125HR Fourier transform spectrometer evacuated at pressures lower than 10^{-4} mbar to avoid absorption by water and residual gas. The ($10 - 60$ cm^{-1}) spectral range has been measured with a resolution of 0.5 cm^{-1} using a 50 microns Mylar beamsplitter combined with a bolometer cooled at 1.6 K having a signal-to-noise ratio of 1700:1. For the ($40 - 600$ cm^{-1}) range, the spectral resolution of 2 cm^{-1} were obtained using a 6 microns Mylar combined with a bolometer cooled at 4.2 K. A low vibration pulse tube cryostat was used to achieve temperatures down to 5 K from room temperature. This system contains a sample holder which is mechanically decoupled from its cold finger, allowing minimum sample vibrations. The absolute reflectance spectra were obtained by measuring the signal reflected in the THz divided by the signal of the gold evaporated sample (see Fig. 1a). Broadband room temperature measurements have been obtained at the SapienzaTerahertz Laboratory at Sapienza University of Rome, through a Vertex 70v FTIR broadband interferometer, for frequencies between 50 and 5000 cm^{-1}, and a JASCO v-770 IR-UV spectrometer for the interval from 3000 to 50000 cm^{-1}. Data obtained from these measurements have been merged to obtain the single broadband reflectance curves (see Fig. 1b).

Acknowledgements

A.A. acknowledges the discussion with L. E. Chow and S. K. Sudheesh and the financial support by the Minsitry of Education MOE), Singapore, under its Tier-2 Academic Research Fund (AcRF), Grant No. MOE-T2EP50121-0018. The authors also thank SOLEIL Synchrotron for providing synchrotron radiation through the project number 20210595. We are thankful to A.

Perrucchi and A. F. Santander-Syro for the guidance in the data treatment and to L. Manceron and K. Rader for the technical support.

Author contributions

The project has been conceptualized and supervised by S.L. and P.R. Samples have been synthesized and characterized by A.A. Infrared measurements were carried out by L.T., R.C., M.V., J.B.B., S.M. and P.R. The data treatment was performed by L.T. and R.C. All authors contributed to the writing of the paper.

Supplementary information

DC Resistance

Fig. S1 shows the DC resistance measurements at various temperatures. The onset of superconductivity near 13 K is clearly visible, as expected from a 0.2 Sr doping.

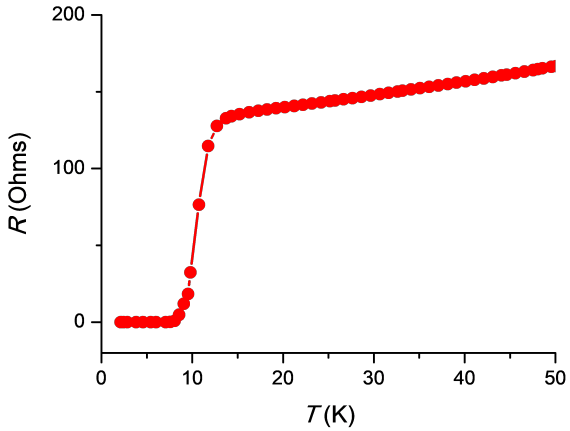

Figure S1. Resistance measurements for various temperatures of 10 nm $Nd_{0.8}Sr_{0.2}NiO_2$/STO. The resistance drops to zero at T $\sim$ 13 K.

Substrate Analisys

The $SrTiO_3$ substrate possesses well known optical features in the low energy spectrum. In particular, due to its incipient ferroelectric nature, a soft phonon mode is expected, with a strong dependence on temperature. This can be seen in Fig. S2, where the absolute reflectance increases at THz frequencies with decreasing temperatures. This is due to the strong red shift of this soft mode. The absolute reflectance of the substrate was fitted using a KK constrained fit of a multi-oscillators Lorentz model thanks to the RefFit software[35]. The substrate optical indices for temperatures below 20 K were then re-integrated inside a multi-layer stacking analysis of the sample (nickelate film) data to remove the contribution of the substrate.

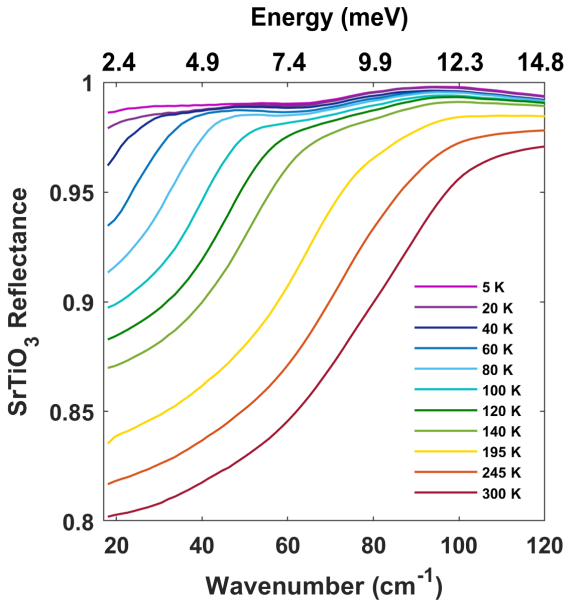

Figure S2. THz reflectance of the $SrTiO_3$ substrate as a function of temperature. The soft phonon mode is clearly shifting toward lower frequencies by decreasing temperature.

ω_p	Γ	ω_0	ω_{pL}	γ
8500	2500	4000	5015	4020

Table S1. Fitting parameters (in cm^{-1}) of Eq. 1 for the Drude and Lorentz oscillators fitting the film conductivity at 300 K.

Superconducting Gap Determination

The Mattis-Bardeen equations (Eq. 2 and 3) are used to extract the superconductive gap by fitting the relative reflectance data shown in Fig. 2a,c and S3a,b. To do this, a series of processes are first required to remove the information coming from the substrate temperature dependence. This is done by computing analytically the expected relative reflectance of a film over substrate through a thin film stacking model[36]. This model takes into account the optical refraction of the substrate as determined by reflectance measurements at the same temperature (see above), the thickness of the film (∼10 nm) and the film conductivity. Inserting the normal state conductivity inside this model gives in output the normal state reflectance computed for the film over substrate at 20 K. Instead, in order to extract the superconductive gap value Δ, we have used a gradient descend algorithm that follows these simple steps:

1. Choose a gap value Δ and a temperature T under analysis
2. Compute the real and imaginary superconductive conductivity through Eq. 2 and 3 (see Fig. S4)
3. Compute the relative reflectance expected for such a film deposited over a STO substrate, as obtained from the thin film stacking model described above
4. Compare the analytical result to the experimental value $\Delta R/R$
5. Calculate a χ^2 value from the comparison
6. Optimize the χ^2 value through a gradient descend algorithm that tunes the parameter Δ
7. Extract the best value $\Delta(T)$ that fits the data

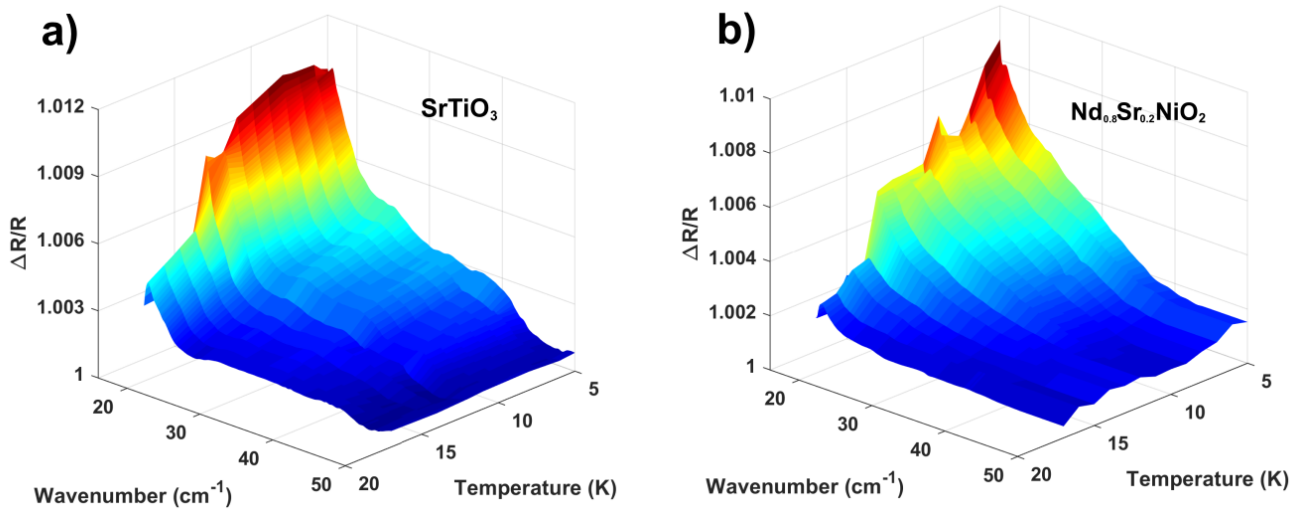

Figure S3. THz relative reflectance measurements of $Nd_{0.8}Sr_{0.2}NiO_2$ and STO substrate as a function of temperature and frequency. The relative heatplots are shown in Fig. 2c,d of the main text.

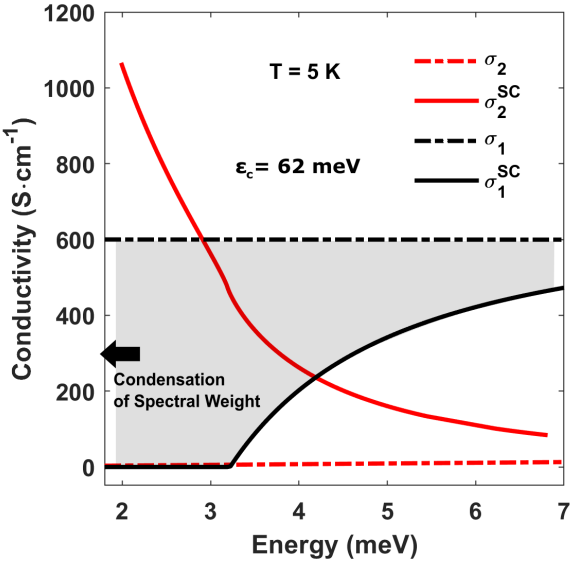

Figure S4. THz plot of the superconductive and normal state optical conductivity of a $Nd_{0.8}Sr_{0.2}NiO_2$ film, as extracted by the Mattis-Bardeen algorithm at 5 K and a Kramers-Kronig constrained fit of the 20 K absolute reflectance, respectively. The grey area highlights the spectral weight difference that is transferred to zero frequency by the Cooper pairs condensation.

References

1. Li, D. *et al.* Superconductivity in an infinite-layer nickelate. *Nature* **572**, 624–627 (2019).

2. Abrikosov, A. A. On the magnetic properties of superconductors of the second group. *Sov. Phys. JETP* **5**, 1174–1182 (1957).

3. Bednorz, J. G. & Mueller, K. A. Possible high T_c superconductivity in the Ba-La-Cu-O system. *Z. Phys. B Condens. Matter* 64, 189–193 (1986).

4. Chaloupka, J. & Khaliullin, G. Orbital order and possible superconductivity in $LaNiO_3$/$LaMO_3$ superlattices. *Phys. Rev. Lett.* **100**, 016404 (2008).

5. Zhang, J. *et al.* Large orbital polarization in a metallic square-planar nickelate. *Nature Phys.* **13**, 864–869 (2017).

6. Anisimov, V. I., Bukhvalov, D. & Rice, T. M. Electronic structure of possible nickelate analogs to the cuprates. *Phys. Rev. B* **59**, 7901–7906 (1999).

7. Hayward, M. A. & Rosseinsky, M. J. Synthesis of the infinite layer Ni(I) phase $NdNiO_{2+x}$ by low temperature reduction of $NdNiO_3$ with sodium hydride. *Solid State Sciences* **5**, 839–850 (2003).

8. Zeng, S. *et al.* Phase diagram and superconducting dome of infinite-layer $Nd_{1-x}Sr_xNiO_2$ thin films. *Phys. Rev. Lett.* **125**, 147003 (2020).

9. Hu, L.-H. & Wu, C. Two-band model for magnetism and superconductivity in nickelates. *Phys. Rev. Research* **1**, 032046 (2019).

10. Liu, Z., Ren, Z., Zhu, W., Wang, Z. & Yang, J. Electronic and magnetic structure of infinite-layer $NdNiO_2$: trace of antiferromagnetic metal. *npj Quantum Mater.* **5**, 1–8 (2020).

11. Kitatani, M. *et al.* Nickelate superconductors—a renaissance of the one-band Hubbard model. *npj Quantum Mater.* **5**, 1–6 (2020).

12. Lechermann, F. Late transition metal oxides with infinite-layer structure: nickelates versus cuprates. *Phys. Rev. B* **101**, 081110 (2020).

13. Werner, P. & Hoshino, S. Nickelate superconductors: multiorbital nature and spin freezing. *Phys. Rev. B* **101**, 041104 (2020).

14. Nomura, Y. *et al.* Formation of a two-dimensional single-component correlated electron system and band engineering in the nickelate superconductor $NdNiO_2$. *Phys. Rev. B* **100**, 205138 (2019).

15. Choi, M.-Y., Lee, K.-W. & Pickett, W. E. Role of $4f$ states in infinite-layer $NdNiO_2$. *Phys. Rev. B* **101**, 020503 (2020).

16. Chen Hanghui, *et al.* Dynamical Mean Field Studies of Infinite Layer Nickelates: Physics Results and Methodological Implications. *Front. Phys. doi: 10.3389/fphy.2022.835942*

17. Zhou, T., Gao, Y. & Wang, Z. Spin excitations in nickelate superconductors. *Sci. China Phys. Mech. Astron.* **63**, 287412 (2020).

18. Giaever, I. Energy Gap in Superconductors measured by electron tunneling. *Phys. Rev. Lett.* **5**, 147–148 (1960).

19. Dressel, M., Wu, D., Barišić, N. & Gorshunov, B. Looking at the superconducting gap of iron pnictides. *Journal of Physics and Chemistry of Solids* **72**, 514–518 (2011).

20. Degiorgi, L., Briceno, G., Fuhrer, M. S., Zettl, A. & Wachter, P. Optical measurements of the superconducting gap in single-crystal K_3C_{60} and Rb_3C_{60}. *Nature* **369**, 541–543 (1994).

21. Morse, R. W. *Progress in Cryogenics* (Heywood and Cy Ltd, London, 220, Vol. I, 1959).

22. Phillips, N. E. Heat capacity of Aluminum between 0.1°K and 4.0°K. *Phys. Rev.* **114**, 676–685 (1959).

23. Warren, W. W., Walstedt, R. E., Brennert, G. F., Espinosa, G. P. & Remeika, J. P. Evidence for two pairing energies from nuclear spin-lattice relaxation in superconducting $Ba_2YCu_3O_{7-\delta}$. *Phys. Rev. Lett.* **59**, 1860–1863 (1987).

24. Chow, L.E.,*et al.* Pairing symmetry in infinite-layer nickelate superconductor *arXiv:2201.10038* (2022)

25. Harvey, S.P., *et al.* Evidence for nodal superconductivity in infinite-layer nickelates *arxiv:2201.12971* (2022)

26. Gu, Q. *et al.* Single particle tunneling spectrum of superconducting $Nd_{1-x}Sr_xNiO_2$ thin films. *Nat. Commun.* **11**, 6027 (2020).

27. Dressel, M. & Drichko, N. Optical properties of two-dimensional organic conductors: signatures of charge ordering and correlation effects. *Chem. Rev.* **104**, 5689–5716 (2004).

28. Basov, D. N. & Timusk, T. Electrodynamics of high-T_c superconductors. *Rev. Mod. Phys.* **77**, 721–779 (2005).

29. Dressel, M., Drichko, N., Gorshunov, B. & Pimenov, A. THz spectroscopy of superconductors. *IEEE Journal of Selected Topics in Quantum Electronics* **14**, 399–406 (2008).

30. Perucchi, A. *et al.* Multiband conductivity and a multigap superconducting phase in films from optical measurements at terahertz frequencies. *Phys. Rev. B* **81**, 092509 (2010)

31. Tinkham, M. *Introduction to Superconductivity* (Mc Graw-Hill, New York, 1996).

32. Timusk, T. & Tanner, D. *Physical Properties of High Temperature Superconductors I* (World Scientific, Singapore, 1989); Timusk, T. & Tanner, D. *Physical Properties of High Temperature Superconductors III* (World Scientific, Singapore, 1992).

33. Peng, W. *et al.* Room-temperature soft mode and ferroelectric like polarization in $SrTiO_3$ ultrathin films: Infrared and *ab initio* study. *Sci Rep* **7**, 2160 (2017).

34. Petzelt, J. *et al.* Dielectric, infrared, and Raman response of undoped $SrTiO_3$ ceramics: Evidence of polar grain boundaries. *Phys. Rev. B* **64**, 184111 (2001).

35. Kuzmenko, A. B. Kramers–Kronig constrained variational analysis of optical spectra. *Review of Scientific Instruments* **76**, 083108 (2005).

36. Heavens, O. S. & Singer, S. F. Optical properties of thin solid films. *Physics Today* **9**, 24–26 (1956).

37. Homes, C. C., Lobo, R. P. S. M., Fournier, P., Zimmers, A. & Greene, R. L. Optical determination of the superconducting energy gap in electron-doped $Pr_{1.85}Ce_{0.15}CuO_4$. *Phys. Rev. B* **74**, 214515 (2006)

38. Congeduti A, *et al.* Infrared study of charge delocalization induced by pressure in the $La_{0.75}Ca_{0.25}MnO_3$ Manganite *Phys. Rev. B* **63**, 184410 (2001)

39. Lupi S., *et al.* Optical conductivity of single crystals of $Na_{0.57}CoO_2$ *Phys. Rev. B* **69**, 180506 (2004)

40. Lo Vecchio I., *et al.* Optical properties of V_2O_3 in its whole phase diagram. *Phys. Rev. B* **91**, 155133 (2015)

41. Degiorgi, L., Electronic correlations in iron-pnictide superconductors and beyond: lessons learned from optics *New Journal of Physics* **13**, 023011 (2011)

42. Yu, Y. *et al.* High-temperature superconductivity in monolayer $Bi_2Sr_2CaCu_2O_{8+\delta}$. *Nature* **575**, 156–163 (2019)

43. Homes, C. C. et al. A universal scaling relation in high-temperature superconductors. *Nature* **430**, 539–541 (2004).

44. Homes, C. C., Dordevic, S. V., Valla, T. & Strongin, M. Scaling of the superfluid density in high-temperature superconductors. *Phys. Rev. B* **72**, 134517 (2005).

45. Tallon, J. L., Cooper, J. R., Naqib, S. H. & Loram, J. W. Scaling relation for the superfluid density of cuprate superconductors: Origins and limits. *Phys. Rev. B* **73**, 180504 (2006).

46. Mattis, D. C. & Bardeen, J. Theory of the anomalous skin effect in normal and superconducting metals. *Phys. Rev.* **111**, 412–417 (1958).

47. Rugheimer, N. M., Lehoczky, A. & Briscoe, C. V. Microwave transmission- and reflection-coefficient ratios of thin superconducting films. *Phys. Rev.* **154**, 414 (1967)

48. Palmer, L. H. & Tinkham, M. Far-infrared absorption in thin superconducting Lead films. *Phys. Rev.* **165**, 588 (1968)

49. Seibold, G., Benfatto, L. & Castellani, C. Application of the Mattis-Bardeen theory in strongly disordered superconductors. *Phys. Rev. B* **96**, 144507 (2017)

50. Gross, F. *et al.* Anomalous temperature dependence of the magnetic field penetration depth in superconducting uranium-beryllium (UBe_{13}). *Z. Phys. B* **64**, 175–88 (1986).

51. Prozorov, R. & Giannetta, R. W. Magnetic penetration depth in unconventional superconductors. *Supercond. Sci. Technol.* **19**, R41–R67 (2006).

52. Dressel, M. & Grüner, G. *Electrodynamics of Solids: Optical Properties of Electrons in Matter* (Cambridge University Press, Cambridge, 2002)

53. Seo, Y., Choi, W., Ahmad, D., Kimura, S. & Kwon, Y. S. Temperature dependence of the superconducting energy gaps in $Ca_{9.35}La_{0.65}(Pt_3As_8)(Fe_2As_2)_5$ single crystal. *Sci. Rep.* **8**, 8648 (2018).

54. Fruchter, L. *et al.* Penetration depth of electron-doped infinite-layer $Sr_{0.88}La_{0.12}CuO_{2+x}$ thin films. *Phys. Rev. B* **82**, 144529 (2010).

55. Bernardini, F., Olevano, V. & Cano, A. Magnetic penetration depth and T_c in superconducting nickelates. *Phys. Rev. Research* **2**, 013219 (2020).

56. Roy, P., Rouzières, M., Qi, Z. & Chubar, O. The AILES Infrared Beamline on the third generation synchrotron radiation facility SOLEIL. *Infrared Physics & Technology* **49**, 139–146 (2006).